Photoassociation of atoms in ultracold collisions probed by wave-packet dynamics

Mette Machholm,[1,2] Annick Giusti-Suzor,[3] and F. H. Mies[4]
[1]*Laboratoire de Photophysique Moléculaire, Bâtiment 213, Université de Paris-Sud, 91405 Orsay Cedex, France*
[2]*Department of Chemistry, H.C. Ørsted Institute, 2100 Copenhagen Ø, Denmark*
[3]*Laboratoire de Chimie Physique, 11 rue Pierre et Marie Curie, 75231 Paris Cedex 05, France*
[4]*National Institute of Standards and Technology, Gaithersburg, Maryland 20899*
(Received 18 July 1994)

Photoassociation in laser-assisted collisions of ultracold alkali atoms has been used recently to perform high-precision spectroscopy of very-long-range states. Rovibrational spectra close to the $Na(3\,^2S)+Na^*(3\,^2P_{3/2})$ dissociation limit have been obtained by monitoring an enhanced Na_2^+ ion signal. We propose the use of pump-probe techniques to study the dynamics of the ionization process. At very large distances (typically 70 a.u.) two colliding Na atoms absorb a photon and form a coherent vibrational wave packet. We follow the packet in time and probe two possible mechanisms that are proposed to yield molecular ions: *photoionization,* where the second photon is absorbed at a small internuclear distance R directly ionizing the molecule, and *associative ionization* with excitation at intermediate R to the nuclear continuum of a doubly excited state followed by a half collision and autoionization at small R. The latter event can also lead to dissociation of the complex. The two mechanisms lead to distinct differences in the ion signals as a function of delay time between the pump and the probe pulses. Estimates of the ion rates to be expected in actual pump-probe experiments are given, which tend to favor the autoionization mechanism as the dominant reaction path.

PACS number(s): 34.50.Rk, 33.80.Eh, 34.50.Gb

I. INTRODUCTION

Photoassociation of laser-cooled alkali atoms [1] recently appeared as a rich source of spectroscopic information on very long-range bound states of alkali dimers [2–4,19], due to the high resolution achievable in the ultracold domain. Photoassociation can be probed by monitoring the fluorescence from excited molecular states, the trap loss signal, or by recording the ionization signal associated with further photon absorption above the ionization threshold of the neutral molecule. In particular, this technique has provided the rovibrational spectra of several long-range states of Na_2 [2(b)], formed by cw laser excitation from colliding pairs of neutral sodium atoms in a magneto-optical trap:

$$Na+Na+h\nu \rightarrow Na_2^* \ . \tag{1}$$

The atom pairs colliding along the ground-state potentials of Na_2, with a relative kinetic energy corresponding to ≈ 0.6 mK ($E=kT$), can reach excited bound states $(1_g,0_u^+,0_g^-)$, which correlate asymptotically to $Na(3\,^2S)+Na(3\,^2P_{3/2})$, by absorption of tunable radiation red-detuned from the atomic resonance transition. Absorption of one more photon from the same laser leads to ionization of the molecule (see Fig. 1):

$$Na_2^*+h\nu \rightarrow Na_2^+ + e^- \ . \tag{2}$$

These observations yield unprecedented spectroscopic data, including hyperfine structure, on long-range states near their dissociation limit, in very good agreement with *ab initio* calculations by Williams and Julienne [5]. However, they provide little information on the mechanism involved in the ionization step (2), which has to occur at short internuclear distance while primary excitation (1) takes place at very long range.

Here we propose a complementary investigation of this

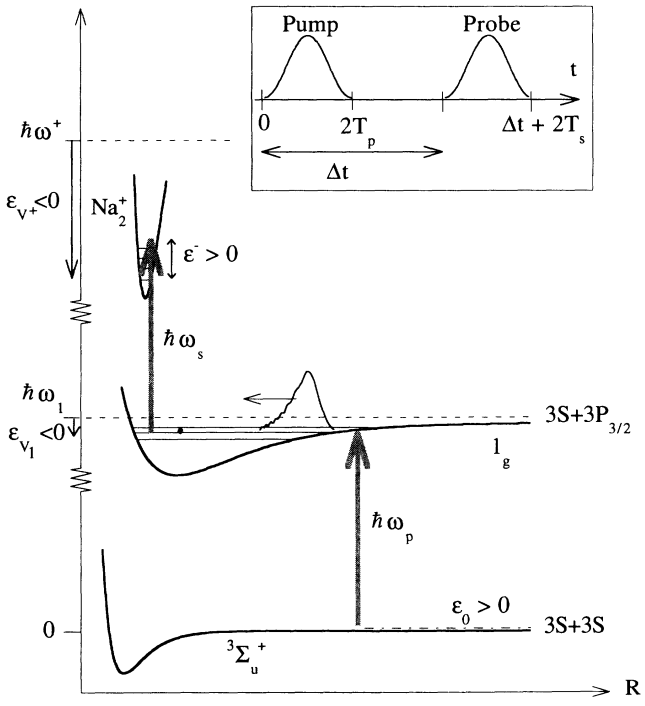

FIG. 1. The pump-probe scheme: photoassociation followed by photoionization. The energy $\hbar\omega_1$ corresponds to the transition $Na(3\,^2P_{3/2}) \rightarrow Na(3\,^2S)$. $\Delta\omega_p=\omega_1-\omega_p \gg \varepsilon_0/\hbar$. The $Na(3\,^2S)+Na(3\,^2S)$ limit is taken as origin for the energy.

photoassociation-ionization process by means of a pump-probe scheme using pulsed lasers. The spectral width associated with short picosecond pulses allows coherent excitation of several rovibrational stationary states with high vibrational quantum numbers. A spatially localized nuclear wave packet is thus formed, and its time evolution can be probed using a second laser pulse delayed in time with respect to the pump pulse. Such pump-probe experiments have provided crucial insight into the dynamics of multistep ionization of the sodium dimer (Baumert *et al.* [6], Engel [7]). Other means to follow the motion of the nuclear wave packet in an excited potential well of sodium dimer have been used, for example, by monitoring the spontaneous emission (Dunn *et al.* [8]). In these experiments, as well as in pioneer experiments in other systems by Zewail and co-workers [9], the wave packet was excited from an initial bound molecule via bound-bound or bound-free transitions to excited states amenable to various probe schemes.

In our case the initial state is a continuum scattering state, and the process is initiated by a free-bound transition to a very anharmonic excited potential. We demonstrate here that at the very low collision energies of the trap, where the energy spread is of the order of $k_B T \approx 6$ MHz, a well localized vibrational wave packet can still be formed in a long-range excited state, long lived enough to be probed by a second laser pulse at various time delays with respect to the pump pulse.

Our main point is to show that such a time-domain analysis can distinguish between two different ionization mechanisms (2) that can occur following the photoassociation process. The first one is direct *photoionization* of the intermediate singly excited state induced by the probe pulse at short internuclear distance, once the wave packet in the 1_g state has reached the Franck-Condon region of the low-lying vibrational levels of the Na_2^+ ground state (Fig. 1). The second ionization scheme proceeds through excitation of the nuclear continuum of a *doubly excited state* of the neutral molecule, asymptotically correlating to $Na(3\,^2P_{1/2})+Na(3\,^2P_{3/2})$ and reached by absorption of a probe photon at intermediate internuclear distance (Fig. 7):

$$Na_2^*(1_g)+h\nu \rightarrow Na_2^{**} \ . \tag{3a}$$

As already studied in the cold collision context by Heather and Julienne [10], such a doubly excited state is electronically coupled at short distance to the ionization continuum and can lead to *associative ionization* (AI) [11] via the autoionization process

$$Na_2^{**} \rightarrow Na_2^+ + e^- \ . \tag{3b}$$

We postulate that the portion of the continuum wave packet associated with Eq. (3a), which initially moves inwards, will experience coupling to the autoionizing channel (3b) and give rise to an ion signal. The part of the continuum wave packet that is not autoionized will lead to dissociation of the neutral molecule:

$$Na_2^{**} \rightarrow Na(3\,^2P_{1/2})+Na(3\,^2P_{3/2}) \ . \tag{3c}$$

We will consider the half-collision process as a weak perturbation to the direct photodissociation process, and predict that a few percent branching into (3b) is sufficient to compete with the photoionization mechanism. It is our purpose to characterize the nuclear wave packet most favorable for associative ionization, and to use the time-delay behavior as a signature to distinguish the collisional ionization signal (3b) from the direct short-range photoionization.

In Secs. II A and II B we first describe the pump step and discuss the effects of various parameters (frequency detuning $\Delta\omega_p$, pulse duration T_p) on the formation and the time evolution of the coherent wave packet in the intermediate singly excited 1_g state, which tends to dominate the photoassociation spectrum in the one-color sodium experiment [2]. Estimates of the total probability of forming such a vibrational wave packet depending on experimental parameters (trap density, laser intensity I_p) are given in Sec. II C. In Secs. III and IV, respectively, we discuss the different probing signals from the two competing processes (2) and (3) leading to ion formation. We also make estimates of the rates to be expected for these two mechanisms. The expressions presented are for a general two-color pump-probe scheme, with independent parameters for the probe pulse (frequency detuning $\Delta\omega_s$, pulse duration T_s, and laser intensity I_s).

Finally, in Sec. V we accumulate the various estimates we have made and simulate a complete pump-probe experiment, using the same photon energy and pulse duration for the pump and probe. We estimate the experimental conditions (trap density, laser detuning, laser intensity, pulse time) that could lead to an ion signal strong enough to be monitored as a function of the time delay between the pump and probe pulses and compare the characteristics of the two proposed mechanisms. Extension to other alkali-atom dimers and implications for the cold atom dynamics will be briefly discussed.

II. PUMP STEP

A. Photoassociation of two Na atoms at long range

The experiment by Lett *et al.* [2] shows that the collisions taking place in the continuum of the $^3\Sigma_u^+$ ground state can lead to photoassociative ionization via the 1_g state (Fig. 1). At the temperatures typically obtained by laser cooling in a magneto-optical trap (MOT, $T < 0.6$ mK) only the first few partial waves of the continuum nuclear motions contribute to the photoassociation. Only s wave scattering is considered in the present model. The rotation is not taken into account, because the spacing of the rotational levels is about 1 GHz compared to the vibrational spacing of about 10 GHz$\approx$0.3 cm^{-1}, giving a corresponding precession time for the rotation which is 10 times larger than for the vibration. In the case of long delay times we might need to include rotation.

In the long-range region where the pump laser induces photoassociation (1) the ground-state potential is nearly flat. We use the extrapolation by Zemke and Stwalley [12] based on the exchange potential and the van der Waals term. The wave packet for a pair of colliding atoms incident on the electronic ground state $|0\rangle$ with

collision energy ε is well represented by the stationary-state energy-normalized continuum wave function:

$$|\Psi_\varepsilon(R,t)\rangle = |0\rangle|\varepsilon(R)\rangle e^{-i\varepsilon t/\hbar} \rightarrow |0\rangle \left[\frac{2\mu}{\hbar^2 \pi k}\right]^{1/2} \times e^{-i\xi_0}\sin(kR+\xi_0)e^{-i\varepsilon t/\hbar}, \quad (4)$$

where $|\varepsilon(R)\rangle$ denotes the elastically scattered nuclear wave function with a phase shift ξ_0. Ideally, we should construct a scattering wave packet with a narrow distribution of incident momenta $\hbar k' \approx \hbar(k \pm \delta)$, but at these ultracold temperatures we can treat each incident energy ε component as an *incoherent wave packet* and will conclude the calculation by performing a thermal average over the final *probabilities*.

In the present perturbative treatment, depletion of the ground state is neglected. The initial state is represented as the quasistationary collisional wave packet in (4), and we assume that the pump pulse only transfers a small fraction of the initial wave packet into an excited bound electronic state, $|1\rangle$:

$$|\Psi_{1\leftarrow\varepsilon}(R,t)\rangle = |1\rangle e^{-i\omega_1 t}\sum_{v_1} c_{v_1\leftarrow\varepsilon}(t)|v_1(R)\rangle e^{-i\varepsilon_{v_1}t/\hbar}. \quad (5)$$

The sum is over the vibrational wave functions $|v_1(R)\rangle$ with energy $\varepsilon_{v_1} < 0$ measured relative to the dissociation limit $\hbar\omega_1$.

The internuclear distance R_p most favorable for photoassociation increases with decreasing detuning $\Delta\omega_p = \omega_1 - \omega_p$, where ω_p is the central frequency of the pump pulse. The internuclear distance R_p can be estimated from the crossing of the excited potential curve and the ground-state potential, the latter dressed by the photon energy $\hbar\omega_p$.

For the long-range excited bound state we use a 1_g adiabatic potential correlating to the $Na(3\,^2S)+Na(3\,^2P_{3/2})$ (Williams and Julienne [5]). Actually, this potential is obtained by diagonalizing the electronic, fine structure, and hyperfine structure interactions in the total angular momentum basis set. At short range this potential correlates to a bound $^1\Pi_g$ potential. Details of this potential have been adjusted based on the spectroscopic measurements of Lett *et al.* [2]. The qualitative results are not too sensitive to minor changes in the potentials, but high-quality potential curves are needed for quantitative comparison with experimental results.

The time-dependent radiative coupling between the ground and the excited states is

$$V_p(t) = \mu_{1\leftarrow 0} E_p \cos(\omega_p t) g_p(t), \quad (6)$$

where E_p is the electric-field amplitude. The dipole moment $\mu_{1\leftarrow 0}$ is assumed to be independent of the internuclear distance and equal to the atomic value. This rough approximation is justified, since only the long-range region contributes to the absorption process. The pseudo-Gaussian pulse shape is given by

$$g_p(t) = \sin^2\left[\frac{\pi t}{2T_p}\right], \quad 0 < t < 2T_p, \quad (7)$$

which is very similar to a Gaussian distribution with half-maximum width T_p, but with the advantage of a well-defined beginning ($t=0$) and end ($t=2T_p$) of the pulse.

By projection of the time-dependent Schrödinger equation on $|1\rangle|v_1\rangle$, we obtain, in the rotating-wave approximation

$$\frac{\partial}{\partial t} c_{v_1\leftarrow\varepsilon}(t) = \frac{E_p}{2i\hbar}\langle v_1|\mu_{1\leftarrow 0}|\varepsilon\rangle e^{i\Omega_{v_1,\varepsilon}t} g_p(t), \quad \Omega_{v_1,\varepsilon} = \Delta\omega_p + \frac{\varepsilon_{v_1}-\varepsilon}{\hbar}. \quad (8)$$

$\Omega_{v_1,\varepsilon}$ is zero when the pump pulse is in resonance with the vibrational level v_1 (see Fig. 1). The expansion coefficients in Eq. (5) are constant for $t \geq 2Tp$:

$$c_{v_1\leftarrow\varepsilon}(2T_p) = C^p_{1\leftarrow 0}\langle v_1|\varepsilon\rangle \int_0^{2T_p} \frac{e^{i\Omega_{v_1,\varepsilon}t}}{iT_p} g_p(t)dt = C^p_{1\leftarrow 0}\langle v_1|\varepsilon\rangle G(\Omega_{v_1,\varepsilon}T_p). \quad (9)$$

The dimensionless quantity $C^p_{1\leftarrow 0}$ measures the coupling strength and is dependent on the peak intensity I_p and the duration T_p of the pulse, and of course the electronic transition moment $\mu_{1\leftarrow 0}$:

$$C^P_{1\leftarrow 0} = \frac{E_p T_p}{2\hbar}\mu_{1\leftarrow 0} \approx 2.7\times 10^{-4}\sqrt{I_p(W/\mathrm{cm}^2)}[T_p(\mathrm{ps})]. \quad (10)$$

Here we have used the atomic value $\mu_{1\leftarrow 0} \approx 2.5$ a.u.

The integral over the pulse shape in Eq. (9) can be expressed as

$$G(X) = \frac{e^{i2X}-1}{2X[(X/\pi)^2-1]}, \quad (11)$$

with $X = \Omega_{v_1,\varepsilon}T_p$. The quantity $|G(X)|^2$ acts as an effective line-shape function for the laser pulse and determines the resonance criterion and the spectral width for the excitation. It exhibits its maximum $|G(0)|^2 = 1$ when $\Omega = 0$. Its full width at half maximum occurs at $X = \pm 2.26$, which predicts a range of excited vibrational energies of the order of $\Delta\varepsilon_{v_1} \approx 4.5\hbar/T_p$.

The evolution of the vibrational wave packet in the 1_g potential will be represented by three-dimensional plots for $t > 2T_p$ as a function of time and internuclear distance R. These are constructed as an incoherent average over a thermal distribution of incident kinetic energies ε, which, because of the threshold behavior ($\varepsilon^{1/4}$) of the matrix elements $\langle v_1|\varepsilon\rangle$ for s waves, can be reduced to a simple expression involving just the mean thermal energy $\epsilon_0 = kT$:

$$|\Psi_1(R,t)|^2 = \int_0^\infty d\varepsilon\, e^{-\varepsilon/kT}|\Psi_{1\leftarrow\varepsilon}(R,t)|^2 \approx |C^p_{1\leftarrow 0}|^2\left[\frac{\sqrt{\pi}}{2}kT\right]W_{1\leftarrow 0}(\epsilon_0,R,t), \quad (12)$$

where

$$W_{1\leftarrow 0}(\varepsilon,R,t)=\sum_{v_1',v_1}\langle v_1|\varepsilon\rangle\langle\varepsilon|v_1'\rangle G^*(\Omega_{v_1,\varepsilon}T_p)G(\Omega_{v_1',\varepsilon}T_p)|v_1(R)\rangle\langle v_1'(R)|e^{i(\varepsilon_{v_1'}-\varepsilon_{v_1})t/\hbar} \tag{13}$$

Such plots (see Figs. 2 and 3) are very useful to follow the dynamics of the wave packet and will be described below.

The derivation of these expressions involve two reasonable assumptions. First we assume that the broadening $\Delta\varepsilon_{v_1}\approx 4.5\hbar/T_p$ due to the laser pulse is very large compared to kT, and we can therefore evaluate the $G(X)$ functions in (13) at their mean energies $\varepsilon_0=kT$ and remove them from the integral. Second, we have also ignored the "broadening" of the upper $|1\rangle|v_1\rangle$ levels due to spontaneous emission, since our pulse duration is much shorter than the radiative lifetime. We have implicitly ignored this effect by treating ε_{v_1} as a discrete energy level rather than a Lorentzian line shape.

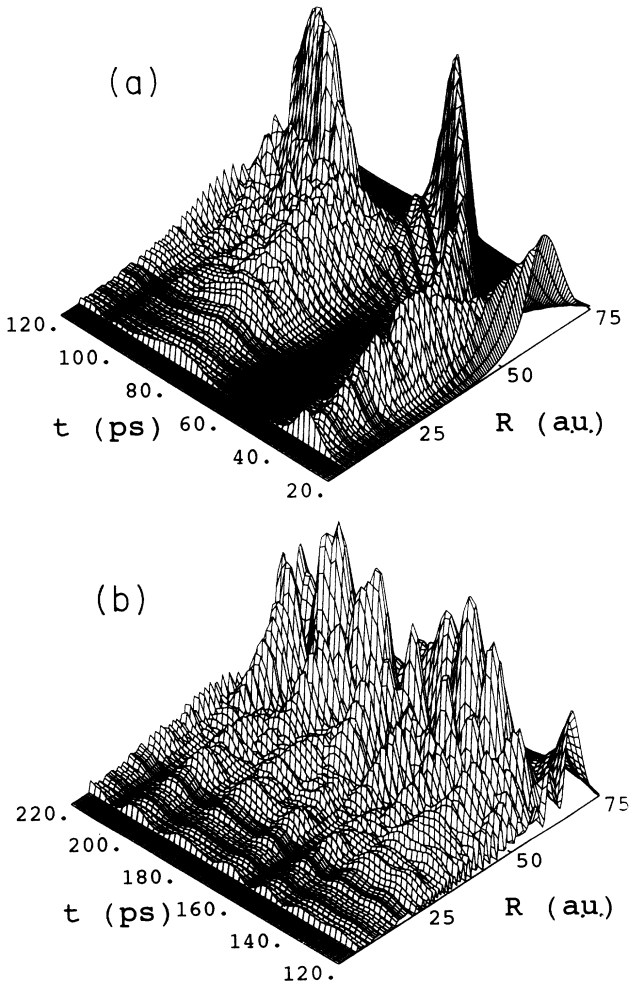

FIG. 2. The evolution of the $v_1\approx 77$ wave packet in the 1_g potential for $\Delta\omega_p/2\pi=180$ GHz and $T_p=10$ ps. (a) The first oscillations in the potential well after the end of the pump pulse at $t=2T_p$; (b) the dispersion of the wave packet in the anharmonic potential.

B. Wave packet in the 1_g state

We have observed that the primary requirement for forming a localized wave packet in the bound-state potential is that the spectral width of the laser pulse Γ_p covers about four vibrational levels. In the relevant units we have

$$\Gamma_p(\mathrm{GHz})\approx\frac{10^3}{T_p(\mathrm{ps})}\ . \tag{14}$$

This implies a duration of the pump pulse T_p, which is about $\frac{1}{4}$ of the oscillation time $T_{\mathrm{osc}}(v_1)=h/\Delta E_{v_1}$ corresponding to the vibrational level spacing $\Delta E_{v_1}=E_{v_1+1}-E_{v_1}$ at the level v_1 in resonance with the central frequency ω_p of the laser pulse. Thereby the wave packet does not move too far during the pump pulse.

In Fig. 2 we show an example of the evolution of a wave packet in the 1_g potential. A well localized wave packet can be obtained for a wide range of laser frequencies by adjusting simultaneously two parameters: the detuning $\Delta\omega_p$ and the pulse duration T_p. Figure 2 corresponds to $\Delta\omega_p/2\pi=180$ GHz, $T_p=10$ ps, and a central vibrational level $v_1\approx 77$. The photoassociation to the 1_g state takes place at large internuclear distance; for example, the wave packet in Fig. 2(a) is formed around $R=65$ a.u. The first oscillation of the wave packet in the potential is clearly seen. The oscillation time of the wave packet (≈ 50 ps in the example) agrees with the oscillation time $T_{\mathrm{osc}}(v_1)$ calculated from the level spacing. The mean velocity of the wave packet is about 2 a.u./ps. The amplitude of the wave packet is about a factor of 10

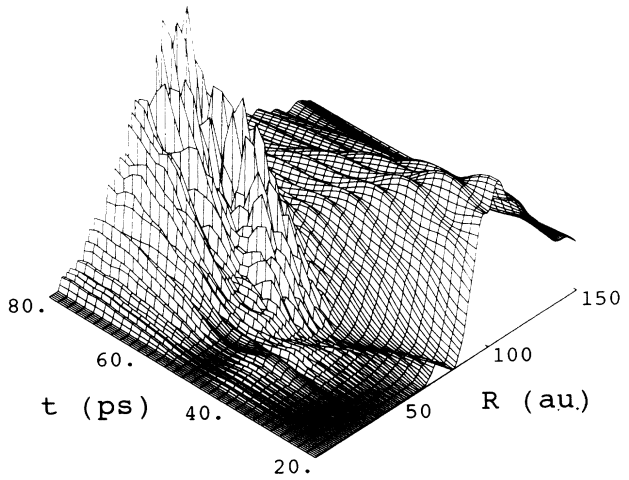

FIG. 3. The first-half oscillation of the $v_1\approx 82$ wave packet in the 1_g potential for $\Delta\omega_p/2\pi=100$ GHz and $T_p=10$ ps, showing the motion of the wave packet towards the inner turning point.

larger at the outer than at the inner turning point. After only a few oscillations the wave packet spreads out [Fig. 2(b)] because the 1_g potential well is very anharmonic. However, we will see in Sec. III that, at longer time, revivals and fractional revivals are observed with the probe schemes.

In the following, we concentrate on the dynamics of the first half oscillation of the wave packet, from the formation at the outer turning until the inner turning point is reached. The above-mentioned requirement $T_p \approx T_{\rm osc}/4$ ensures a well-localized wave packet, which does not spread out too fast. This requirement also implies that the wave packet will reach the inner turning point shortly after the end of the pump pulse, $t = 2T_p$. Therefore, any scheme probing the wave packet at small or intermediate internuclear distance will give the first maximum in the probe signal around the minimum delay between the pump and the probe pulse, $\Delta t = 2T_p$.

If we are only interested in the dynamics during the first half oscillation of the wave packet, it does not matter that the wave packet spreads out for $t > T_{\rm osc}/2$. Therefore, we can violate the requirement $T_p \approx T_{\rm osc}/4$, as for example in Fig. 3 where the detuning is only 100 GHz giving $T_{\rm osc} \approx 88$ ps, keeping $T_p = 10$ ps. The $v_1 \approx 82$ wave packet is formed at $R_p > 85$ a.u. At the end of the pump pulse the front of the wave packet is at $R = 75$ a.u. The inner turning point is reached at $t \approx 4T_p$. In Sec. III B a probe signal corresponding to this type of the wave packet is discussed.

The most important limitation for obtaining a "well-behaved" wave packet comes from the Franck-Condon factors for the continuum $\rightarrow$ bound transition. Even for a set of parameters $\Delta\omega_p$ and T_p fulfilling $T_p \approx T_{\rm osc}/4$, the wave packet can be inadequate for probing the dynamics. This is the case if the Franck-Condon factor is minimum for a vibrational level in resonance with the central frequency (the minima arise from nodes in the initial continuum wave function). The wave packet will then split into two parts corresponding to excitation in the wings of the pump pulse. These parts oscillate with different frequencies in the bound potential.

C. Estimate of rates

The total probability *per pump pulse,* that a given quasimolecule is pumped into the manifold of excited vibrational levels, is obtained by integration of Eq. (12) over R:

$$P_{1\leftarrow 0} = |C^p_{1\leftarrow 0}|^2 \left[\frac{\sqrt{\pi}}{2} kT \sum_{v_1} |\langle v_1|\varepsilon_0\rangle|^2 |G(\Omega_{v_1,\varepsilon_0} T_p)|^2 \right] \quad (t > 2T_p) , \tag{15}$$

$$\approx 1.6\times 10^{-10} [I_p(\mathrm{W/cm^2})][T_p(\mathrm{ps})]^2 .$$

This estimate is obtained by summing over four vibrational levels, with $|G|^2 \approx \frac{1}{2}$, and taking the typical value $|\langle v_1|\varepsilon_0\rangle|^2 \approx 0.1\ \mathrm{GHz}^{-1}$ ($T = 0.6$ mK).

The total density of quasimolecules (accessible for pumping) formed by the thermal collision of $Na(^2S)+Na(^2S)$ atoms incident on the ground $^3\Sigma_u^+$ electronic state with incident nuclear angular moment l and azimuthal projection m_l is

$$\rho_0^{\max} = \frac{\omega_{^3\Sigma} N_A^2}{2Q_{\rm tr}(T)\omega_A^2} = 3.5\times 10^{-18}\ \mathrm{cm^3}\times N_A^2 . \tag{16}$$

We have used the electronic degeneracy of the $Na(^2S)$ ground-state atom $\omega_A = 2$, the degeneracy of the incident molecular electronic state $\omega_{^3\Sigma} = 3$, and the translational partition function $Q_{\rm tr} = (2\pi\mu kT/h^2)^{3/2}$. Note that the density will increase as the square of the atom density N_A in the trap, a crucial parameter in the experiments.

III. FIRST PROBE MECHANISM: DIRECT PHOTOIONIZATION AT SMALL INTERNUCLEAR DISTANCE

A. Photoionization of the vibrational wave packet

At short internuclear distance (8–10 a.u.) direct photoionization of the $Na_2^*(1_g)$ is possible with a second photon of the same wavelength as for the pump step (Fig. 1). This mechanism is a good candidate for probing the motion of the wave packet in the 1_g potential, since the primary criterion for obtaining a probe signal, which depends on the delay between the two pulses Δt, is a localized transition to the probe state.

In a one-color experiment, where the central frequency of the probe pulse ω_s equals ω_p, only the first four vibrational levels $|v^+(R)\rangle$ of the ion ground state $|0^+\rangle$ are energetically allowed (see Fig. 1). The resulting wave function for the photoionization (PI) is

$$|\Psi_{\mathrm{PI}\leftarrow\varepsilon}(R,t)\rangle = \int d\varepsilon^- e^{-i(\omega^+ + \varepsilon^-)t/\hbar} |0^+,\varepsilon^-\rangle \times \sum_{v^+} |v^+(R)\rangle e^{-i\varepsilon_{v^+} t/\hbar} c_{v^+,\varepsilon^-}(t) . \tag{17}$$

The sum is over the vibrational levels v^+, with the energy ε_{v^+} relative to the dissociation limit $\hbar\omega^+$ of $Na_2^+(\varepsilon_{v^+} < 0)$. The radiative coupling can be expressed as for the pump step [Eq. (6)], with the electric-field amplitude E_s. The temporal shape is given as in Eq. (7) with the pulse length T_s. We use the potential-energy curve of the Na_2^+ ground state calculated by Meyer [13].

The total wave function is the sum of vibrational wave packet $\Psi_{1\leftarrow\varepsilon}$ [Eq. (5)], which we assume is only weakly perturbed by the probe laser, and this ionized component $\Psi_{\mathrm{PI}\leftarrow\varepsilon}$. Inserting it into the time-dependent Schrödinger equation and projecting onto $|v^+\rangle|\varepsilon^-\rangle|0^+\rangle$, gives, in the rotating-wave approximation,

$$\frac{\partial}{\partial t} c_{v^+,\varepsilon^-} = \frac{E_s}{2i\hbar} \sum_{v_1} \langle v^+|\mu_{0^+,\varepsilon^-\leftarrow 1}|v_1\rangle c_{v_1\leftarrow\varepsilon}(t) \times e^{i\Omega_{v^+,\varepsilon^-,v_1} t} g_s(t-\Delta t) , \tag{18}$$

$$\Omega_{v^+,\varepsilon^-,v_1} = \omega^+ - \omega_1 - \omega_s + (\varepsilon_{v^+} - \varepsilon_{v_1} + \varepsilon^-)/\hbar .$$

The transition is prevalent when $\Omega_{v^+,\varepsilon^-,v_1} \to 0$. This "near energy-conserving" condition selects the range for the energy of the ejected electron ε^- for given vibrational levels of Na_2^* and Na_2^+. We may also assume that the ε^- variation of the photoionization transition dipole $\mu_{0^+,\varepsilon^-\leftarrow 1}(R)=\langle 0^+,\varepsilon^-|\mu|1\rangle$ is negligible over the pulse width, and further that it is essentially independent of R in the region of the equilibrium ion distance, which contributes most to the overlap integrals $\langle v^+|v_1\rangle$. In this perturbative treatment the expansion coefficients $c_{v_1\leftarrow\varepsilon}(2T_P)$ are taken to be constant and given by Eq. (9), as determined at the end of the pump pulse. With these approximations the PI expansion coefficients become at the end of the probe pulse

$$c_{v^+,\varepsilon^-}(\Delta t+2T_s)=C^S_{0^+,\varepsilon^-\leftarrow 1}\sum_{v_1} e^{i\Omega_{v^+,\varepsilon^-,v_1}\Delta t}\langle v^+|v_1\rangle c_{v_1\leftarrow\varepsilon}(2T_p)G(\Omega_{v^+,\varepsilon^-,v_1}T_S)\ , \tag{19}$$

where integration again yields the line-shape factor $G(\Omega_{v^+,\varepsilon^-,v_1}T_s)$ as defined in Eq. (11). Unlike the dimensionless quantity in Eq. (10), the square of the radiative coupling strength,

$$|C^S_{0^+,\varepsilon^-\leftarrow 1}|^2=\left|\frac{E_s}{2}\mu_{0^+,\varepsilon^-\leftarrow 1}\right|^2\left[\frac{T_s}{\hbar}\right]^2=\left[\frac{2\pi I_s}{c}\right]\left|\mu_{0^+,\varepsilon^-\leftarrow 1}\right|^2\left[\frac{T_s}{\hbar}\right]^2\ , \tag{20}$$

now has dimensions of inverse energy due to the energy normalization of the electron continuum. The more useful quantity to evaluate is the photoionization rate times T_s, as predicted by the usual golden rule expression (see Fano and Rau [14]):

$$P^S_{0^+,\varepsilon^-\leftarrow 1}=\frac{2\pi}{\hbar}\left|\frac{E_s}{2}\mu_{0^+,\varepsilon^-\leftarrow 1}\right|^2 T_s=\frac{8\pi^3}{\lambda_s}\left|\mu_{0^+,\varepsilon^-\leftarrow 1}\right|^2\frac{I_s}{\hbar\omega_s}T_s\ , \tag{21a}$$

$$P^S_{0^+,\varepsilon^-\leftarrow 1}=\sigma_{0^+,\varepsilon^-\leftarrow 1}\frac{I_s}{\hbar\omega_s}T_s\approx 3.0\times 10^{-12}[I_s(\mathrm{W/cm^2})][T_s(\mathrm{ps})]\ . \tag{21b}$$

Here we have used the estimate $\sigma\approx 10^{-18}$ cm^2 for the photoionization cross section [15] and the Na($3S\to 3P$) resonance energy $\hbar\omega_s\approx 0.077$ a.u.

The observable quantity is the total ion signal as a function of the delay between the pump and the probe pulses, $P^+_{\mathrm{PI}}(\Delta t)$. This implies an integration over the energy of the ejected electron and a summation over the vibration levels of the Na_2^+ ion, as well as an integration over the thermal distribution of incident ground-state kinetic energies ε:

$$\begin{aligned}P^+_{\mathrm{PI}}(\Delta t)&=\int d\varepsilon^-\int_0^\infty d\varepsilon\, e^{-\varepsilon/kT}\sum_{v^+}|c_{v^+,\varepsilon^-}(\Delta t+2T_p)|^2\\&=|C^P_{1\leftarrow 0}|^2P^S_{0^+,\varepsilon^-\leftarrow 1}\left[\frac{\sqrt{\pi}}{2}kT\right]\int\frac{d\varepsilon^-T_s}{2\pi\hbar}\sum_{v^+}\left|\sum_{v_1}\langle v^+|v_1\rangle\langle v_1|\varepsilon_0\rangle e^{-i\varepsilon_{v_1}\Delta t/\hbar}G(\Omega_{v_1,\varepsilon_0}T_p)G(\Omega_{v^+,\varepsilon^-,v_1}T_s)\right|^2\ .\end{aligned} \tag{22}$$

The number of molecular ions produced at the completion of the probe pulse is obviously a function of the delay time and it is this dependence that we hope to exploit in characterizing the photoionization mechanisms.

B. Time-delay behavior of direct photoionization mechanism

In the present calculations the pump and the probe pulses have the same central frequency $\omega_p=\omega_s$ and the same length, $T_p=T_s$. In Fig. 4 the ion signal is shown as a function of the delay Δt. It probes the wave-packet motion in the 1_g bound state, more precisely at the inner turning point around which photoionization can occur. Indeed, the maxima in the ion signal are observed for time delays $\Delta t=(n+\frac{1}{2})T_{\mathrm{osc}}(v_1)$. The first maximum is a factor of 100 larger than the first minimum.

The most striking features are the revivals and fractional revivals of the ion signal [16]. Due to the anharmonicity of the potential well the wave packet spreads out after a few oscillations, giving less pronounced minima and maxima in the ion signal. For longer time the relative phase of two vibrational levels matches the initial relative phase modulo 2π, and the wave packet is again localized. The revival time T_{rev} of the wave packet may be estimated by a simplified four-level formula [6(b), 16(a)]:

$$T_{\mathrm{rev}}=\frac{h}{2E_{v_1}-E_{v_1+1}-E_{v_1-1}}\ . \tag{23}$$

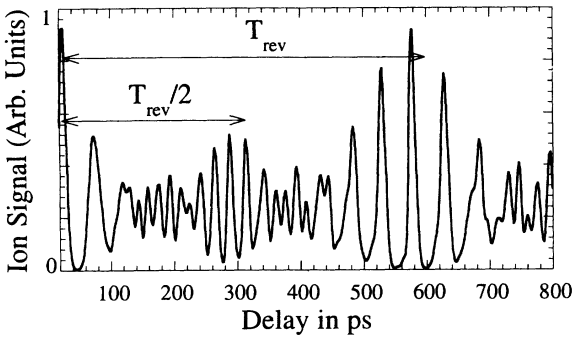

FIG. 4. The production of Na_2^+ ions as a function of the delay Δt between the pump and the probe laser pulses. $\Delta\omega_p/2\pi=\Delta\omega_s/2\pi=180$ GHz, $T_p=10$ ps. The $\frac{1}{2}$ fractional revival and the full revival of the ion signal are seen at $t=T_{\rm rev}/2$ and $T_{\rm rev}$, respectively.

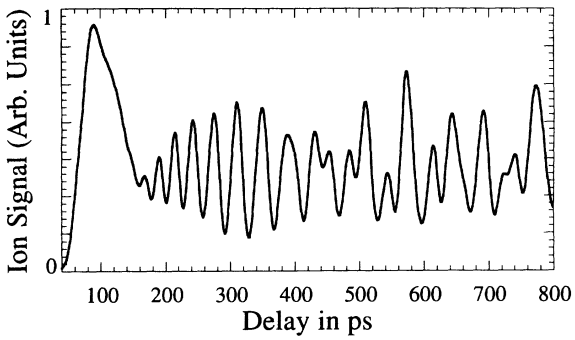

FIG. 5. The production of Na_2^+ ions as a function of the delay Δt between the pump and the probe laser pulses. $\Delta\omega_p/2\pi=\Delta\omega_s/2\pi=50$ GHz, $T_p=20$ ps. With these parameters about ten vibrational levels centered around $v_1\approx 88$ contribute to the wave packet.

In the ion signal the revival is observed by reconstruction of the initial peak pattern.

A fractional revival at $\Delta t\approx T_{\rm rev}/2$ is clearly seen in Fig. 4, characterized by the ion signal that peaks with twice the initial frequency. This fractional revival corresponds to a splitting of the wave packet in two parts, as seen for atomic Rydberg wave packets [16(a)].

Figure 5 shows the ion signal corresponding to a wave packet with more than four vibrational levels included. With $\Delta\omega_p/2\pi=\Delta\omega_s/2\pi=50$ GHz and $T_p=20$ ps about ten levels are excited. Even in this case a clear delay-time dependence is seen in the ion signal, though the signal is not as regular as in the case of a "four-level" wave packet.

As discussed in Sec. II, the ion signal for wave packets fulfilling $T_p\approx T_{\rm osc}/4$ has a maximum for the minimum delay time $\Delta t=2T_p$, because the wave packet reaches the inner turning point shortly after the end of the pump pulse. Figure 6 shows ion signals for wave packets formed with pulses where $T_p<T_{\rm osc}/4$, corresponding to different detunings $\Delta\omega_p$. The first maximum in each ion signal probes the time the front of the wave packet uses to travel from R_p to the inner turning point.

C. Order of magnitude of the direct photoionization signal

As a rough measure of the magnitude of the expected ion signal we use the average of $P_{\rm PI}^+(\Delta t)$ [Eq. (22)] over Δt, which is essentially equivalent to ignoring the cross terms in the v_1 summation. We then obtain

$$\langle P_{\rm PI}^+(\Delta t)\rangle_{\rm av}\approx|C^P_{1\leftarrow 0}|^2 P^S_{0^+,\varepsilon^-\leftarrow 1}\left[\frac{\sqrt{\pi}}{2}kT\right]\left[\frac{3}{4}\right]\sum_{v^+}\sum_{v_1}|\langle v^+|v_1\rangle\langle v_1|\varepsilon_0\rangle G(\Omega_{v_1}T_p)|^2 \tag{24}$$

The factor $\frac{3}{4}$ comes from the integral of $\int_0^\infty dX|G(X)|^2=3\pi/2$. Assuming that the magnitude of $\langle v^+|v_1\rangle$ for a given v^+ is insensitive to the range of v_1, we can use Eq. (15) to express (24) as follows:

$$\langle P_{\rm PI}^+(\Delta t)\rangle_{\rm av}=P_{1\leftarrow 0}\langle P_{\rm ion}(\Delta t)\rangle_{\rm av}\ , \tag{25a}$$

$$\langle P_{\rm ion}(\Delta t)\rangle_{\rm av}\approx P^S_{0^+,\varepsilon^-\leftarrow 1}\left[\frac{3}{4}\right]\left\langle\sum_{v^+}|\langle v^+|v_1\rangle|^2\right\rangle_{\rm av}$$

$$\approx 1.1\times 10^{-14}[I_s({\rm W/cm^2})][T_s({\rm ps})]\ . \tag{25b}$$

In (25b) we have used the estimates in Eq. (21b) and taken the averaged sum over the Franck-Condon factors to be of the order of 5×10^{-3} for the sodium dimer system.

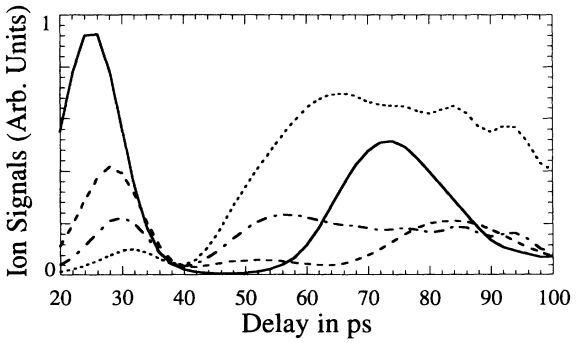

FIG. 6. The dynamics of the first-half oscillation reflected in the ion signal. $T_p=10$ ps. ——, $\Delta\omega/2\pi=180$ GHz; — — —, $\Delta\omega/2\pi=140$ GHz; —·—·—·, $\Delta\omega/2\pi=120$ GHz; and · · · ·, $\Delta\omega/2\pi=100$ GHz.

The peak value of (22) for proper delay times might be as much as 5 to 10 times larger than the value found in (25b) due to constructive interference.

IV. SECOND PROBE MECHANISM: AUTOIONIZATION OF SHORT DISTANCES AFTER PHOTON ABSORPTION AT INTERMEDIATE INTERNUCLEAR DISTANCES

A. Initial step: Creation of a wave packet in the nuclear continuum of a doubly excited state

The amplitude of the wave packet in the 1_g state, Fig. 2, is *much* smaller at the inner turning point than at intermediate and large internuclear distances R. Therefore it is relevant to study competing ionization mechanisms by a scheme that probes the wave packet at intermediate R. We propose here a two-step probe scheme (Fig. 7): (i) The excitation at intermediate R into the nuclear continuum of a doubly excited state [Eq. 3(a)], which correlates asymptotically to $Na(3\,^2P_{3/2})+Na(3\,^2P_{1/2})$. (ii) The resulting wave packet "performs" a half collision, which can lead to autoionization at small R [Eq. 3(b)]. In a one-color experiment this probe scheme is only possible for detunings smaller than half the fine-structure splitting $\hbar\omega_{FS}$ of the $Na(3\,^2P)$. For larger detunings the energy of two photons is too small to reach the doubly excited state.

Several doubly excited states of Na_2 are known to cross the ion ground state in the Franck-Condon region of the lowest vibrational levels (Dulieu *et al.* and Weiner, Masnou-Seeuws, and Giusti-Suzor [11]) and to correlate to $Na(3\,^2P)+Na(3\,^2P)$ with a R^{-5} long-range behavior (Heather and Julienne [10]). This flat behavior of the potential compared to the 1_g curve (C_3/R^3 at large R) gives a well-localized excitation region R_s, which is the main criterion for obtaining a delay-time-dependent probe signal. We have chosen a potential with $R_s \approx 55$ a.u. estimated from the crossing of the doubly excited potential and the 1_g potential dressed with one photon of energy $\hbar\omega_s$.

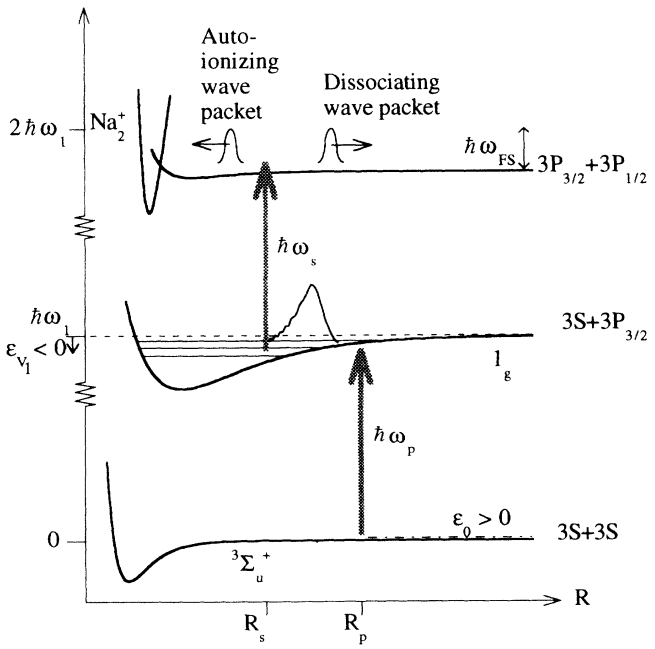

FIG. 7. The second probe scheme: photoassociation and excitation to the nuclear continuum of a doubly excited state, and possible autoionization. The wave packet is probed at intermediate distance R_s.

The initial step in this indirect ionization is the excitation to the nuclear continuum of the doubly excited state, $|2\rangle$. The wave function is given by

$$|\Psi_{2\leftarrow\varepsilon}(R,t)\rangle = |2\rangle e^{-i\omega_2 t}\int d\varepsilon_2 c_{\varepsilon_2}(t)|\varepsilon_2(R)\rangle e^{-i\varepsilon_2 t/\hbar}, \tag{26}$$

with ε_2 being the relative kinetic energy of the Na nuclei. The radiative coupling to the 1_g bound state has the same form as in Eq. (6), with a dipole moment assumed to have the atomic value since the excitation takes place at very long range.

Inserting the wave function $|\Psi_{1\leftarrow\varepsilon}(R,t)\rangle + |\Psi_{2\leftarrow\varepsilon}(R,t)\rangle$ into the time-dependent Schrödinger equation, projecting onto $|\varepsilon_2(R)\rangle|2\rangle$ and integrating, gives

$$\frac{\partial}{\partial t}c_{\varepsilon_2} = \frac{E_s}{2i\hbar}\sum_{v_1}\langle\varepsilon_2|\mu_{2\leftarrow 1}|v_1\rangle e^{i\Omega_{\varepsilon_2,v_1}t} c_{v_1\leftarrow\varepsilon}(t) g_s(t-\Delta t), \tag{27}$$

$$\Omega_{\varepsilon_2,v_1} = \omega_2-\omega_1-\omega_s+(\varepsilon_2-\varepsilon_{v_1})/\hbar = \Delta\omega_s-\omega_{FS}+(\varepsilon_2-\varepsilon_{v_1})/\hbar .$$

$\hbar\omega_{FS}$ is the fine-structure splitting between the Na $(3\,^2P_{1/2})$ and $Na(3\,^2P_{3/2})$. $\Omega_{\varepsilon_2,v_1}$ is again a resonance criterion which selects the energy ε_2 reached in the nuclear continuum from the level v_1.

In the perturbative treatment the expansion coefficients $c_{v_1\leftarrow\varepsilon}$ are taken to be constant and given by (9), determined at the end of the pump pulse. In the following it is assumed that the pump and the probe pulse do not overlap in time, $\Delta t > 2T_p$. With these approximations the expansion coefficients become at the end of the probe pulse

$$c_{\varepsilon_2}(\Delta t+2T_s) = C^S_{2\leftarrow 1} e^{i(\Delta\omega_s-\omega_{FS}+\varepsilon_2/\hbar)\Delta t} \times\sum_{v_1}\langle\varepsilon_2|v_1\rangle c_{v_1}(2T_p) \times e^{-i\varepsilon_{v_1}\Delta t/\hbar} G(\Omega_{\varepsilon_2,v_1}T_s), \tag{28}$$

where the integration again yields the line-shape factor $G(\Omega_{\varepsilon_2,v_1}T_s)$ as defined in Eq. (11). The radiative coupling strength takes the same form as (10), i.e.,

$$C^S_{2\leftarrow 1} = \frac{E_s T_s}{2\hbar}\mu_{2\leftarrow 1} \approx 2.7\times 10^{-4}\sqrt{I_s(\mathrm{W/cm^2})}\,T_s(\mathrm{ps}) \tag{29}$$

with the atomic value for the dipole moment $\mu_{2\leftarrow 1}\approx 2.5$ a.u.

The probe pulse excitation forms a thermally averaged wave packet in the nuclear continuum of the doubly excited state (Fig. 7), with a form similar to Eq. (12):

$$|\Psi_2(R,t)|^2=|C^S_{2\leftarrow 1}|^2|C^P_{1\leftarrow 0}|^2\left[\frac{\sqrt{\pi}}{2}kT\right]$$
$$\times\left|\int d\varepsilon_2 e^{i\varepsilon_2(\Delta t-t)/\hbar}|\varepsilon_2(R)\rangle\sum_{v_1}\langle\varepsilon_2|v_1\rangle\langle v_1|\varepsilon_0\rangle e^{i\varepsilon_{v_1}\Delta t/\hbar}G(\Omega_{v_1,\varepsilon_0}T_p)G(\Omega_{\varepsilon_2,v_1}T_s)\right|^2 . \quad (30)$$

The total probability $P_{2\leftarrow 0}(\Delta t)$ for excitation into the double-continuum can be derived from (30) and is, of course, dependent on the delay time for the onset of the probe pulse:

$$P_{2\leftarrow 0}(\Delta t)=|C^S_{2\leftarrow 1}|^2|C^P_{1\leftarrow 0}|^2\left[\frac{\sqrt{\pi}}{2}kT\right]\int d\varepsilon_2\left|\sum_{v_1}\langle\varepsilon_2|v_1\rangle\langle v_1|\varepsilon_0\rangle e^{i\varepsilon_{v_1}\Delta t/\hbar}G(\Omega_{v_1,\varepsilon_0}T_p)G(\Omega_{\varepsilon_2,v_1}T_s)\right|^2 . \quad (31)$$

B. Delay-time dependence of the autoionization signal

In this section we divide the probability in Eq. (31) into an incoming and outgoing component:

$$P_{2\leftarrow 0}(\Delta t)=P^{\text{in}}_{2\leftarrow 0}(\Delta t)+P^{\text{out}}_{2\leftarrow 0}(\Delta t) , \quad (32)$$

and assume that the incoming portion has a certain probability P_2^+ of undergoing an inelastic coupling to the associative ionization channel:

$$P^+_{\text{AI}}(\Delta t)\approx P_2^+ P^{\text{in}}_{2\leftarrow 0}(\Delta t) . \quad (33)$$

However, in order to appreciate the half-collision character of this two-step mechanism, we first examine the spatial and temporal behavior of the wave packet in Eq. (30).

In Fig. 8 we show the motion of the continuum wave packet, originating from a $v_1\approx 79$ vibrational wave packet, for three different values of the delays Δt between the pump and the probe pulses. The detuning is $\Delta\omega_p/2\pi=\Delta\omega_s/2\pi=140$ GHz and pulse length $T_p=15$ ps. In Fig. 8(a) the main part of the continuum wave packet starts moving towards smaller internuclear distances R. Thereby the molecular complex might undergo autoionization forming Na_2^+. If the complex is not autoionized it will dissociate at later times, when it moves back out. In Fig. 8(b) the continuum wave packet moves directly outwards only leading to dissociation of the complex. For some delay times the continuum wave packet splits into two parts, one part moving outwards, the other inwards, as in Fig. 8(c). The motion of the wave packet in the 1_g bound potential is transferred to the continuum wave packet; if for example the bound wave packet is moving toward smaller R, the continuum wave packet will also start out in this direction. The total amount of excitation to the nuclear continuum also depends on Δt. Thus both the different cases of motion and the total amount of excitation ensure a delay-time-dependent ion signal in this probe scheme.

To estimate the delay-time dependence of the ion signal in this scheme, we integrate over R the inward and outward moving parts of the continuum wave packet separately. Thereby we obtain an estimate of $P^{\text{in}}_{2\leftarrow 0}(\Delta t)$ and $P^{\text{out}}_{2\leftarrow 0}(\Delta t)$.

The probe distance R_s changes very little with the detuning. For instance, when varying $\Delta\omega/2\pi$ from 30 to 250 GHz, R_s *increases* from 52 to 63 a.u. However, in the same interval of detunings the pump distance R_p de-

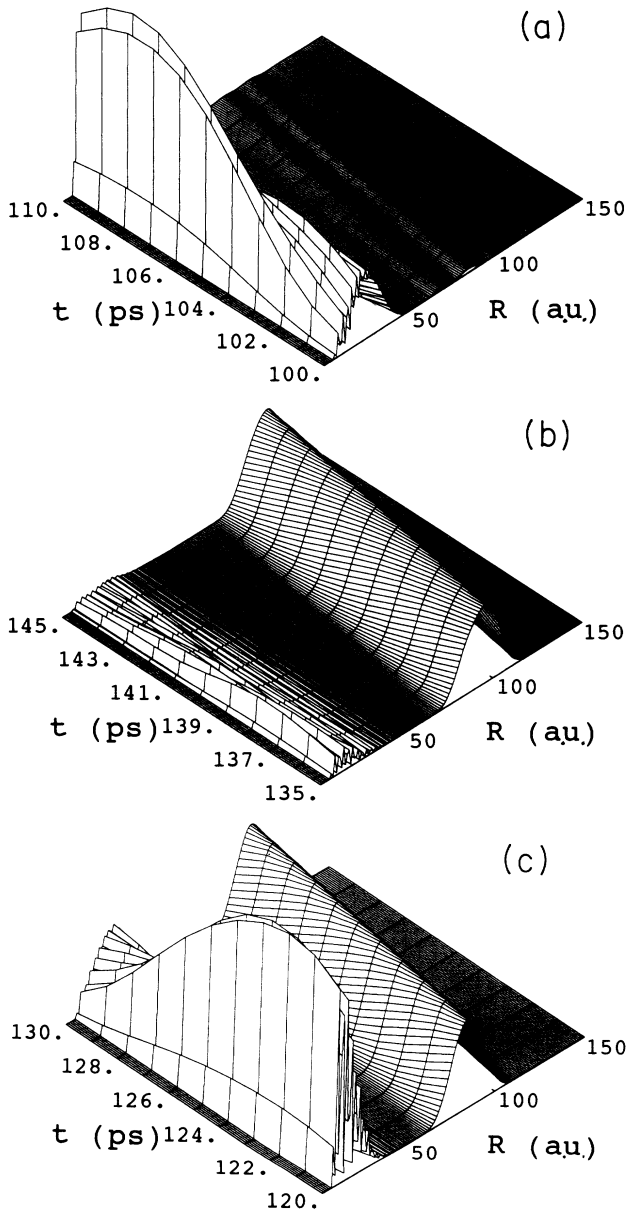

FIG. 8. Wave packet in the nuclear continuum, $\Delta\omega_p/2\pi=\Delta\omega_s/2\pi=140$ GHz and $T_p=T_s=15$ ps. (a) $\Delta t=40$ ps, inward motion; (b) $\Delta t=75$ ps, mainly outward motion; (c) $\Delta t=60$ ps, the wave packet split in two parts, one moving inwards and the other outwards.

creases rapidly from 131 to 64 a.u. For small detunings we therefore find the first maximum in the ion signal for a delay time $T_{\rm osc}/4 < \Delta t < T_{\rm osc}/2$. Indeed, the maxima in the second scheme's probe signal are found for delay times being $T_{\rm osc}/4$ smaller than the delay times for the corresponding maxima in the first scheme's probe signal. For small detunings we find that the second scheme also probes the motion of the wave packet in the 1_g state, giving the same spread and revivals of the wave packet. An example of the different delay-time dependence of the two probe signals is given in Fig. 9.

At small detunings the wave packet in the 1_g state does not have the time to move to the second excitation region during the pump pulse. But for large detunings where $R_s \approx R_p$ the absorption of two photons during the pump pulse should be considered. Absorption of two photons from a single pulse will give rise to an ion signal, which is independent of the delay time, and this is thus an undesirable effect. We have evaluated the probability of the continuum→bound and bound→continuum transition to take place during one laser pulse, and find that for small detunings (30–140 GHz) this signal is much smaller than the delayed excitation signal. For larger detunings ($\approx$200 GHz) the two-photon absorption becomes important.

To conclude, this scheme provides a delay-time-dependent ion signal for small detunings. For larger detunings, close to half the fine-structure splitting, the delay-time dependence of the ion signal disappears due to the delay-time independent contribution from the two-photon absorption during one pulse.

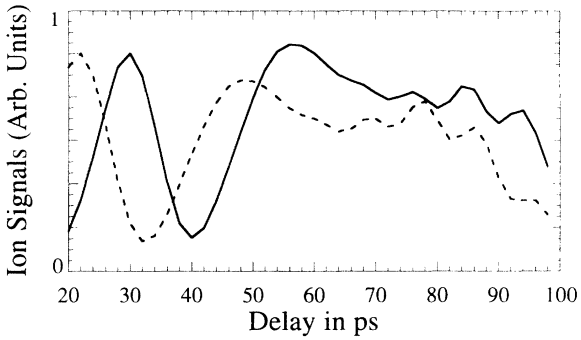

FIG. 9. Comaprison of the delay-time dependence of the two ion signals, normalized to the same peak maximum. ——, the photoionization scheme; — — —, the autoionization scheme. $\Delta\omega/2\pi = 120$ GHz, $T_p = T_s = 10$ ps.

C. Order of magnitude of the autoionization signal

As we did in Eq. (24) for the first probe scheme, we can obtain a rough measure of the total excitation probability by averaging over the possible delay times in (31),

$$\langle P_{2\leftarrow 0}(\Delta t)\rangle_{\rm av} \approx |C^S_{2\leftarrow 1}|^2 |C^P_{1\leftarrow 0}|^2 \left[\frac{\sqrt{\pi}}{2} kT\right] \left[\frac{2\pi\hbar}{2T_s}\right] \sum_{v_1} |\langle \varepsilon_2|v_1\rangle\langle v_1|\varepsilon_0\rangle G(\Omega_{v_1,\varepsilon_0} T_p)|^2 \ . \tag{34}$$

The matrix elements $\langle \bar{\varepsilon}_2|v_1\rangle$ vary significantly with the kinetic energy of the doubly excited continuum ε_2, and in the estimate we use a mean $|\bar{v}_1\rangle$ and a mean value of $|\langle \varepsilon_2|v_1\rangle|^2$ centered around $\bar{\varepsilon}_2 \approx \omega_{\rm FS} - \Delta\omega_s - \Delta\omega_p$, giving

$$\langle P_{2\leftarrow 0}(\Delta t)\rangle_{\rm av} \approx \langle P_{2\leftarrow 1}(\Delta t)\rangle_{\rm av} P_{1\leftarrow 0} \ , \tag{35a}$$

$$\langle P_{2\leftarrow 1}(\Delta t)\rangle_{\rm av} \approx |C^S_{2\leftarrow 1}|^2 \left[\frac{3\pi\hbar}{2T_s} |\langle \bar{\varepsilon}_2|\bar{v}_1\rangle|^2\right] \approx 5.5\times 10^{-5} [I_s({\rm W/cm^2})][T_s({\rm ps})][|\langle \bar{\varepsilon}_2|\bar{v}_1\rangle|^2({\rm GHz^{-1}})] \ . \tag{35b}$$

Estimates of $|\langle \varepsilon_2|v_1\rangle|^2$ range from 10^{-1}–10^{-5} GHz^{-1}, depending on the detunings of the pump and the probe pulses.

It is interesting to compare the continuum→bound absorption $P_{1\leftarrow 0}$ in Eq. (15) to the bound→continuum absorption $\langle P_{2\leftarrow 1}(\Delta t)\rangle_{\rm av}$ in (35b). We find that the second transition probability is about a factor of 10 larger than the first one, with the typical values $T_p = T_s = 10$ ps and $|\langle \bar{\varepsilon}_2|\bar{v}_1\rangle|^2 \approx 0.0005$ GHz^{-1}. This reflects the fact that the initial thermal distribution of continuum states contributing to $P_{1\leftarrow 0}$ is narrow compared to the laser bandwidth and greatly diminishes the initial absorption into the intermediate state $|1\rangle$.

V. COMPETITION BETWEEN THE TWO IONIZATION PROBE SCHEMES

In this section we discuss the magnitude of the ion signal that can be expected in an experiment, based on our estimates for $P_{1\leftarrow 0}$, $\langle P_{\rm ion}(\Delta t)\rangle_{\rm av}$ and $\langle P_{2\leftarrow 1}(\Delta t)\rangle_{\rm av}$ [Eqs. (15), (25b), and (35b)].

In a MOT with a density $N_A = 10^{11}$ cm^{-3} and a volume $V = 10^{-3}$ cm^3 we have [Eq. (16)] $V\rho_0^{\rm max} = 35$ quasimolecules accessible for pumping into the manifold of excited vibrational states *per pump pulses.* The estimate is for an incident partial wave $l = 0$. Including p and d partial waves increases the available population by factors of

$(2l+1)$, or $1+3+5=9$.

Let us now estimate the laser intensity I_p required to pump a significant percentage of the quasimolecules into the vibrational wave packet. At a detuning of $\Delta\omega_p/2\pi=50$ GHz ($v_1\approx 88$) about four vibrational levels are accessed with a pulse length of $T_p=20$ ps. Inserting into (15) we get $P_{1\leftarrow 0}\approx 7\times 10^{-8}(I_p)$ (W/cm^2). Thus to obtain a few percent we need a peak intensity of the order of $I_p=10^6$ W/cm^2. In that case we get $P_{1\leftarrow 0}\approx 0.07$, and 7% of the quasimolecules will be pumped into the excited-state wave packet, giving about $0.07\times 35=2$ molecules per pulse. Assuming a very generous laser repetition rate of 10^7/s, that means about 2×10^7 molecules per second should be formed. With the given parameters for the pump pulse and focused to an area of 10^{-2} cm^2 a powerful pump laser of 2-W average output would be necessary, and for weaker, more realistic lasers the ion signal will be reduced accordingly.

For the estimates for the two competing ionization mechanisms we use the same parameters for the pump and the probe pulses, $I_p=I_s=10^6$ W/cm^2 and $T_p=T_s=20$ ps. Inserting into (25b) we get for the photoionization process $\langle P_{\rm ion}(\Delta t)\rangle_{\rm av}\approx 2\times 10^{-7}$; thus about four molecular ions per second in average. With a favorable delay time for the probe this might be enhanced by a factor of 5 to yield 20 ions per second, and of course our estimates of the relevant cross sections and transition dipoles is very crude, so additional factors of 10 or so in either direction are easily allowed. However, even given these uncertainties we must conclude that the experimental conditions for observing the direct photoionization mechanism are just at the thin edge of feasibility.

On the other hand, when inserting into (35b) we get a probability for excitation into the nuclear continuum per probe pulse $\langle P_{2\leftarrow 1}(\Delta t)\rangle_{\rm av}$, which can approach 100%. This is seven orders of magnitude larger than the estimated direct photoionization probability. Of course one question still remains: the size of the autoionizing probability P_2^+ in (33). However, unless P_2^+ is negligible, which is hardly expected, we anticipate that this indirect mechanism will be vastly more productive of ions than the direct mechanism. With the above laser parameters we estimate that 10^7 P_2^+ molecular ions might be produced per second, and we have appreciable latitude to reduce the pump-probe intensities to less demanding values and still achieve experimentally attractive ion signals.

In conclusion, we expect the one-color pump-probe experiment with Na in a MOT to give a delay-time-dependent ion signal for small detunings via the dominating autoionization mechanism. As the detuning is increased, the delay-time dependence disappears due to two-photon absorption from one pulse, with pump and probe excitations at the same internuclear distance. When the detuning is increased further, the ion signal drops dramatically because the excitation to the doubly excited continuum becomes energetically forbidden at $\Delta\omega\approx\omega_{\rm FS}/2$ and only the photoionization mechanism remains. This qualitative behavior is actually observed in the present c.w. experiments [17]. The photoionization mechanism gives a delay-time-dependent ion signal at all detunings, but might be too weak to be experimentally observable.

The present time-domain analysis of photoassociation of ultracold Na followed by ionization shows information complementary to that obtained in spectroscopy with cw lasers. The Na system is appropriate for studying the competition of the two ionization mechanisms with the one-color pump-probe schemes above, since the lowest vibrational levels of the Na_2^+ can be reached with twice the photon energy needed in the photoassociation excitation. Time-domain analysis of other alkali-metal-atom systems (e.g., Rb) might be more favorable for experiments, primarily because higher average laser power is available (e.g., Ti:sapphire) for their ground state$\rightarrow$ photoassociative state transition. However, for these alkali-atom systems two-color pump-probe schemes are required since a more energetic probe photon is needed to reach doubly excited states correlating to higher atomic levels. We can easily adapt the present perturbative calculations to other alkali-atom systems. With higher laser power it might be necessary to use nonperturbative calculations, taking into account lower state depletion and stimulated emission [18].

Pump-probe analysis provides a fruitful insight into the dynamics of binary ultracold collisions. Such analysis should be helpful for understanding more complex processes occurring in traps with higher density (cluster formation, Bose-Einstein condensation), certainly among the most promising developments of ultracold experiments.

ACKNOWLEDGMENTS

The authors thank Professor J. Weiner for helpful discussions. They also wish to thank Dr. P. Julienne and Dr. C. Williams for providing the potential curve for the 1_g state. One of us (M.M.) acknowledges the foundation of Her Royal Majesty, the Queen Margrethe II, and His Highness, the Prince Henrik, and the Danish Research Academy for financial support. This work was supported in part by a NATO grant for International Collaborative Research.

[1] H. R. Thorsheim, J. Weiner, and P. S. Julienne, Phys. Rev. Lett. **58**, 2420 (1987).

[2] (a) P. D. Lett, K. Helmerson, W. D. Phillips, L. P. Ratliff, S. I. Rolston, and M. E. Wagshul, Phys. Rev. Lett. **71**, 2200 (1993); (b) L. P. Ratliff, M. E. Wagshul, P. D. Lett, S. L. Rolston, and W. D. Phillips, J. Chem. Phys. **101**, 2638 (1994).

[3] V. Bagnato, L. Marcarsa, C. Tsao, Y. Wang, and J. Weiner, Phys. Rev. Lett. **70**, 3225 (1993).

[4] J. D. Miller, R. A. Cline, and D. J. Heinzen, Phys. Rev. Lett. **71**, 2204 (1993).

[5] C. J. Williams and P. S. Julienne, J. Chem. Phys. **101**, 2634

(1994).

[6] (a) T. Baumert, M. Grosser, R. Thalweiser, and G. Gerber, Phys. Rev. Lett. **67**, 3753 (1991); (b) T. Baumert, V. Engel, C. Röttgermann, W. T. Strunz, and G. Gerber, Chem. Phys. Lett. **191**, 639 (1992).

[7] V. Engel, Chem. Phys. Lett. **178**, 130 (1991).

[8] T. J. Dunn, J. N. Sweetser, I. A. Walmsley, and C. Radzewics, Phys. Rev. Lett. **70**, 3388 (1993).

[9] R. M. Bowman, M. Dantus, and A. H. Zewail, Chem. Phys. Lett. **161**, 297 (1989); E. D. Potter, J. L. Herek, S. Pedersen, Q. Liu, and A. H. Zewail, Nature **355**, 66 (1992).

[10] R. W. Heather and P. S. Julienne, Phys. Rev. A **47**, 1887 (1993).

[11] J. Weiner, F. Masnou-Seeuws, and A. Giusti-Suzor, Adv. At. Mol. Phys. **26**, 209 (1990); O. Dulieu, A. Giusti-Suzor, and F. Masnou-Seeuws, J. Phys. B **24**, 4391 (1991); O. Dulieu, S. Magnièr, and F. Masnou-Seeuws, Z. Phys. (to be published).

[12] W. T. Zemke and W. C. Stwalley, J. Chem. Phys. (to be published).

[13] W. Meyer (unpublished).

[14] U. Fano and A. R. P. Rau, *Atomic Collisions and Spectra* (Academic, New York, 1986), Chap. 2.

[15] Using a rough estimate of the ionization rate [extracted from the photoionization data for H calculated by A. Giusti-Suzor and P. Zoller, Phys. Rev. A **36**, 5178 (1987)] in Eq. (21a) predicts $|\mu_{0^+,\varepsilon^-\leftarrow 1}$ (a.u.) $|^2=2a_0^3$. From Eq. (21) we can relate the photoionization cross section and photoionization transition dipole as follows: $|\mu|^2 \equiv[\lambda(a_0)][\sigma(a_0^2)]/(8\pi^3)=3.373(a_0^3)[\sigma(10^{-18}$ cm$^2)]/[\hbar\omega$ (eV)], which gives $\sigma\approx 10^{-18}$ cm^2.

[16] (a) I. Sh. Averbukh and N. F. Perelman, Phys. Lett. A **139**, 449 (1989); (b) Z. Dačić Geata and C. R. Stroud, Jr., Phys. Rev. A **42**, 6308 (1990); D. R. Meacher, P. E. Meyler, I. G. Hughes, and P. Ewart, J. Phys. B **24**, L63 (1991).

[17] P. Lett (private communication).

[18] M. Sell and W. Domcke, J. Chem. Phys. **95**, 7806 (1991).

[19] W. I. Alexander, E. R. I. Abraham, N. W. M. Ritchie, C. J. William, H. T. C. Stoll, and R. G. Hulet (unpublished).

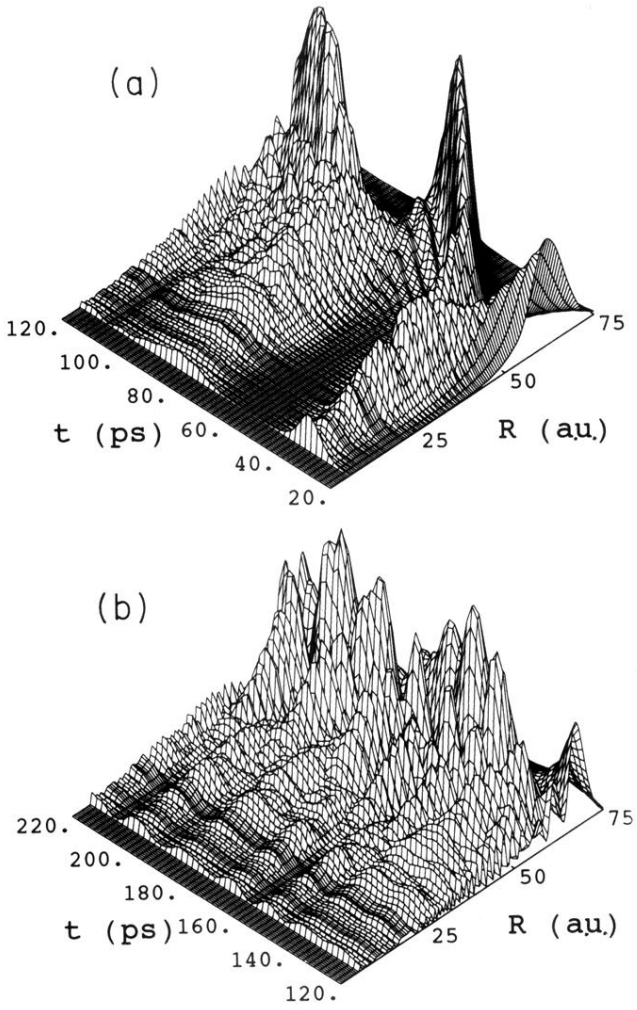

FIG. 2. The evolution of the $v_1 \approx 77$ wave packet in the 1_g potential for $\Delta\omega_p/2\pi = 180$ GHz and $T_p = 10$ ps. (a) The first oscillations in the potential well after the end of the pump pulse at $t = 2T_p$; (b) the dispersion of the wave packet in the anharmonic potential.

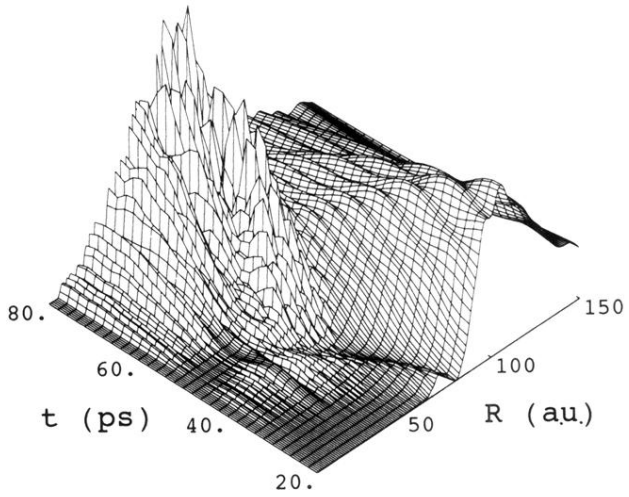

FIG. 3. The first-half oscillation of the $v_1 \approx 82$ wave packet in the 1_g potential for $\Delta\omega_p/2\pi = 100$ GHz and $T_p = 10$ ps, showing the motion of the wave packet towards the inner turning point.

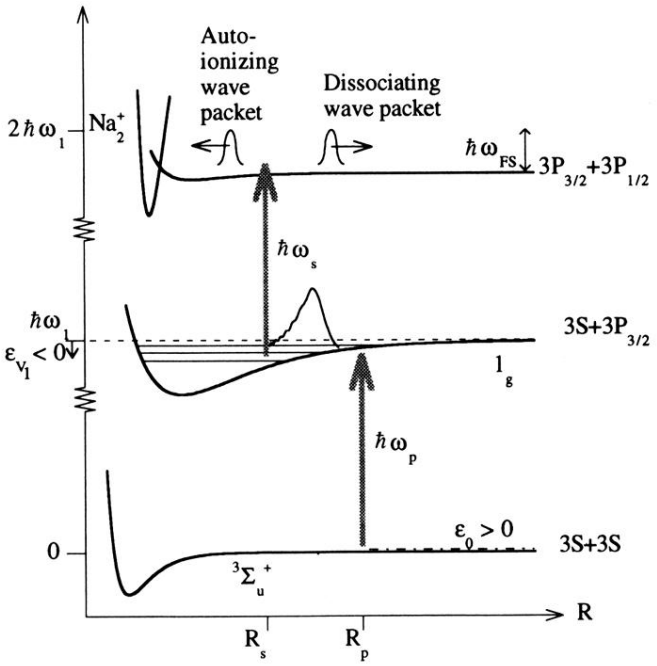

FIG. 7. The second probe scheme: photoassociation and excitation to the nuclear continuum of a doubly excited state, and possible autoionization. The wave packet is probed at intermediate distance R_s.

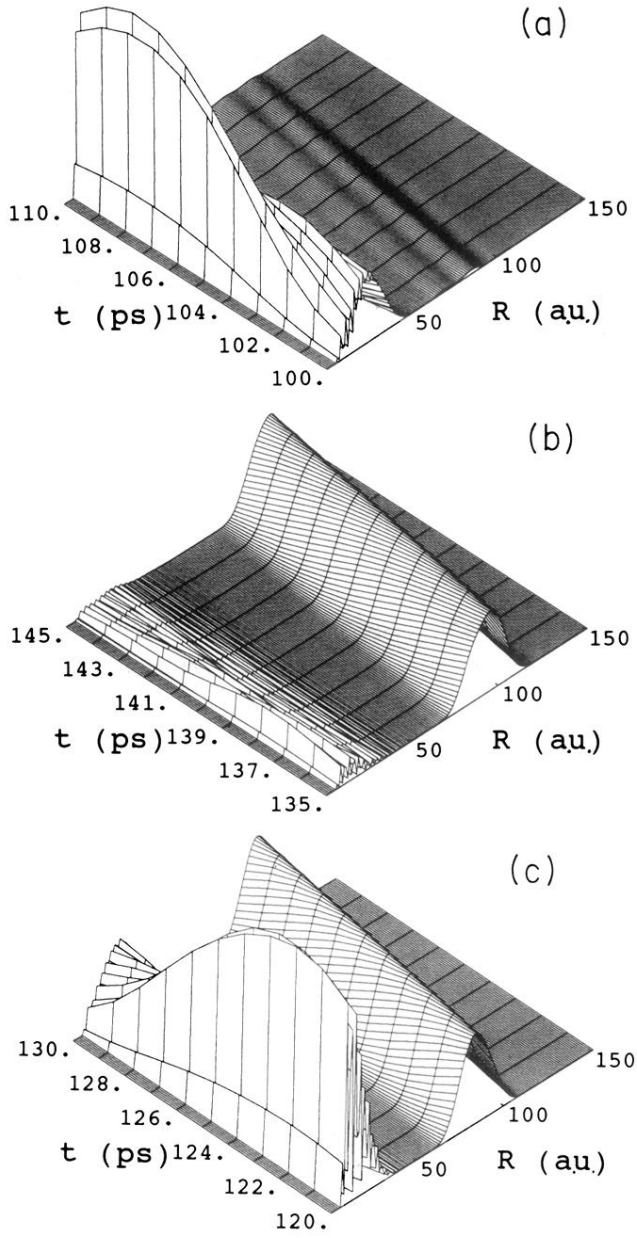

FIG. 8. Wave packet in the nuclear continuum, $\Delta\omega_p/2\pi = \Delta\omega_s/2\pi = 140$ GHz and $T_p = T_s = 15$ ps. (a) $\Delta t = 40$ ps, inward motion; (b) $\Delta t = 75$ ps, mainly outward motion; (c) $\Delta t = 60$ ps, the wave packet split in two parts, one moving inwards and the other outwards.